Composites: Part A 143 (2021) 106315

Contents lists available at ScienceDirect

Composites Part A

journal homepage: www.elsevier.com/locate/compositesa

A numerical approach to characterize the viscoelastic behaviour of fibre beds and to evaluate the influence of strain deviations on viscoelastic parameter extraction

Vincent Werlen [a,b,*], Christian Rytka [a], Véronique Michaud [b]

[a] Institute of Polymer Engineering (IKT), University of Applied Sciences and Arts Northwestern Switzerland (FHNW), CH-5210 Windisch, Switzerland
[b] Laboratory for Processing of Advanced Composites (LPAC), Institute of Materials (IMX), École Polytechnique Fédérale de Lausanne (EPFL), CH-1015 Lausanne, Switzerland

ARTICLE INFO

Keywords:
A. Fabrics/textiles
B. Mechanical properties
C. Analytical modelling
D. Mechanical testing

ABSTRACT

The development of a robust material model able to accurately describe fibre bed compaction at different strain and strain rates is highly desirable because it is essential for the simulation of many composite manufacturing processes. In this study, we investigate the validity of an analytical viscoelastic model approach for different fabrics and at a wide range of strains, both in dry and wet conditions. We propose a numerical approach to determine the parameters of the material model that can overcome simplifications usually met with analytical approaches. We show that a three-branches Maxwell model with strain dependent stiffness and strain-rate dependent dampers can accurately describe the viscoelastic compaction behaviour of fibre beds at different strains and strain speeds, both in dry and wet conditions. We demonstrate that strain deviations have a considerable impact on the viscoelastic parameter extraction and should be taken into account.

1. Introduction

During manufacturing of fibre-reinforced composites the fibre bed will usually be compacted to increase the fibre volume fraction and to improve the part mechanical properties. The modelling of several manufacturing techniques such as Compression Resin Transfer Moulding (CRTM) [1,2], Resin Film Infusion (RFI) [3–5] or direct thermoplastic melt impregnation [6,7] requires knowledge about the fibre bed stress response.

The description of the mechanical behaviour of fibre textiles has been and is still an active research topic as witnessed by the rich literature dealing with this matter [8–21]. During the compaction of a stack of textiles the fibres are pressed together and act as elastic bending beams. Fibres and tows slide past each other to rearrange themselves, causing friction forces. The resulting nesting of the fibres and fibre bundles is thereby influenced by the lubrication of the textile. These combined effects result in a complex viscoelastic behaviour [22].

The characterization of fibre beds is no trivial task and significantly different results can be obtained with the same material depending on the testing equipment and methodology. The first international benchmark exercise on textile permeability and compressibility characterization highlighted that the main source of variation is uncertainty in the measurement of the cavity height [23], mainly due to machine compliance. To counteract this effect, methods such as that presented by Sousa and al., which presented an indirect thickness measurement method, can be applied to identify and eliminate errors in cavity height measurement [24]. During the characterization of fibre beds, several effects will cause a deviation between the prescribed and the measured strain. These different effects are listed below together with the terminology that is adopted in this article:

- **Machine compliance:** The compliance of the testing machine itself leads to errors in cavity height measurements. This is usually corrected on the basis of an empty compaction curve.
- **Machine deflection:** As the applied force decreases during relaxation, the machine deformation decreases as well, which induces a change in cavity height. This behaviour was reported by Sousa and al. [24] and could significantly impact the results but has been neglected by the analytical approach adopted by many authors.
- **Actuation error:** The deviation between the prescribed and measured cavity height caused by the controller inaccuracy. This effect especially takes place at the start and end of a compaction

* Corresponding author at: Laboratory for Processing of Advanced Composites (LPAC), Institute of Materials (IMX), École Polytechnique Fédérale de Lausanne (EPFL), CH-1015 Lausanne, Switzerland.
E-mail address: vincent.werlen@epfl.ch (V. Werlen).

https://doi.org/10.1016/j.compositesa.2021.106315
Received 6 October 2020; Received in revised form 21 January 2021; Accepted 23 January 2021
Available online 3 February 2021

because the control of the machine needs to react to the measured force values.

In this article, we adopt a numerical approach to determine the parameters of the material model that can overcome simplifications usually met with analytical approach and consider machine deflection and actuation error which are usually neglected. This methodology is applied to the three-branches Maxwell recently proposed by Danzi [18]. We investigate its validity for different fabrics at a wide range of strains and strain rates in both dry and wet conditions. Finally, we investigate the impact of neglecting machine deflection during parameter extraction on the quality of the results.

1.1. State of the art

Early models only considered the elastic response of the fibre beds. In 1946, Van Wyk modelled the compression behaviour of wool with bending beams [8]. Several authors subsequently proposed models based on the same assumption, such as Gutowski [25] or Toll [19] who considered different types of assembly following a micromechanical approach.

However, fibre beds display a pronounced viscoelastic behaviour and soon time-dependent models were proposed. This matter was commonly described with rheological models consisting of a combination of spring and dampers, usually a generalized Maxwell model. Also known as the Maxwell–Wiechert model, it consists of a spring placed in parallel with an arbitrary number of spring-dashpot elements called Maxwell elements. Kim and McCarthy [20] were the first to describe the relaxation of fibre textiles with this model in 1991, using a linear model with five spring-dashpot elements.

In further studies several Maxwell models were proposed with a different number of branches and nonlinear springs to describe the quasi-static response of the textile [11] or strain-dependent parameters [10], following the findings of Bickerton et al. [22] who found that the time dependent response of fibre beds depends on the strain and compaction rate. More recently, Danzi et al. [18] proposed a three-branches Maxwell model with strain-dependent springs and strain-rate dependent dashpots, which was found to give good results over a wide range of strains and strain speeds. However, this model was only verified with one dry textile so that its performance with different textiles remains to be proven both in dry and wet conditions.

1.2. Approach

We are interested in developing an efficient model that can be applied for different fabrics under both dry and wet conditions, at a wide range of fibre volume fractions including very high compaction levels, which are for example relevant for composite manufacturing methods such as CRTM, film stacking [4] or direct thermoplastic melt impregnation [6,7]. The approach and methodology adopted here initially follows that proposed by Danzi [18]. Therefore, we consider a variant of the Maxwell model with three branches as shown in Fig. 1: an elastic branch with strain dependent stiffness $E_0(\epsilon)$, three viscoelastic branches with strain dependent stiffnesses $E_1(\epsilon)$, $E_2(\epsilon)$, $E_3(\epsilon)$ and strain-rate dependent relaxation times $\tau_1(\dot{\epsilon})$, $\tau_2(\dot{\epsilon})$ and $\tau_3(\dot{\epsilon})$ where the subscript indicates to which branch the parameter belongs to. The branches are sorted with increasing order of relaxation time so that the first, second and third branches are responsible respectively for the short-, middle- and long-term response of the fibre bed.

The different models presented above generally rely on an analytical approach considering a linear generalized Maxwell model to derive nonlinear parameters. In this study, we investigate the use of a finite difference numerical approach in order to improve the data analysis, and to quantify the impact of some simplifications usually taken in the analytical approach, such as the assumption of a perfectly constant strain during a relaxation experiment. For the parameter extraction

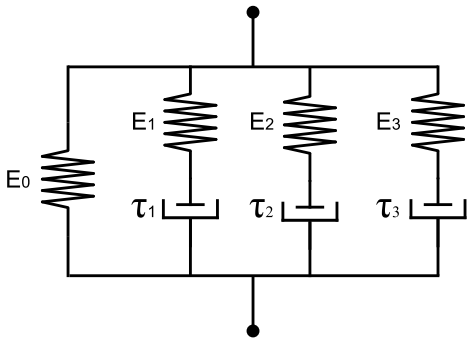

Fig. 1. Schematic representation of a Maxwell model with three branches. The elastic branch is characterized by a single spring on the left while the viscoelastic branches consist of a spring and damper in series.

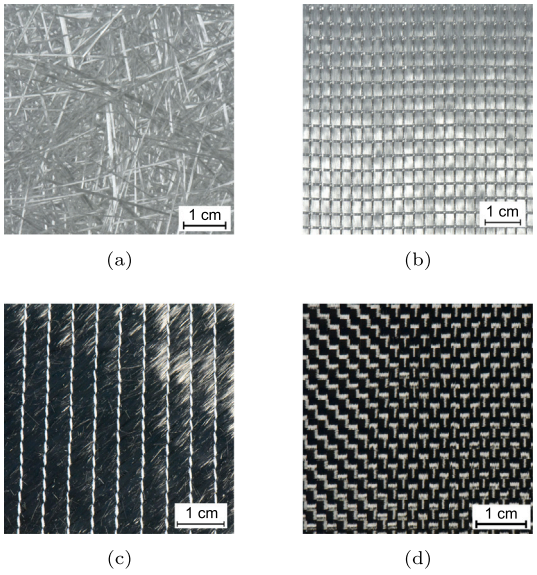

Fig. 2. Pictures of the different textiles used for the experiments.

we consider small compaction steps and approximate the viscoelastic branches behaviour as linear but consider a non-linear elastic branch. The compaction history of the textile is neglected and we assume that the superposition principle for multiple steps functions can be applied to derive model parameters.

2. Materials and methods

2.1. Materials

Different textile architectures based either on glass or carbon yarns have been considered to evaluate the performance of the model on a broad range of materials. Four different textiles were selected and tested in this study: a chopped glass fibres mat shown in Fig. 2(a), a quasi-unidirectional (UD) glass weave shown in Fig. 2(b), a biaxial carbon non-crimp fabric with +/−45° fibre orientation shown in Fig. 2(c) and a carbon plain weave shown in Fig. 2(d). For each of these fabrics the areal weight was measured with a scale while the density of the fabric was measured with the buoyancy method using a Kern precision scale with an immersion set-up, three samples were tested for both methods.

2.2. Experimental test setup

Single plies were cut to squares with a side length of 175 mm using a CNC cutting machine. The plies were then laid with an orientation

Table 1
Overview of the multiple compaction step procedure. The 5N corresponds to the preload at the beginning of the test.

Step nr.	Maximum force [kN]	Maximum stress [Pa]	Holding time [s]
–	5e−3	349	0
0	20e−3	1397	30
1	0.1	6.99 e^3	500
2	0.2	1.40 e^4	500
3	0.3	2.10 e^4	500
4	1	6.99 e^4	500
5	2	1.40 e^5	500
6	3	2.10 e^5	500
7	10	6.99 e^5	1000
8	15	1.05 e^6	1000
9	20	1.40 e^6	1000
10	40	2.79 e^6	1000
11	60	4.19 e^6	1000
12	95	6.64 e^6	1000

of 0° to form a stack, whereby the number of plies is chosen for each material such that the total thickness is approximatively 13 mm in uncompressed state. Each textile was tested in both dry and wet conditions with a Zwick Roell Z100 universal testing machine. The sample is placed between two steel plates with a diameter of 135 mm as shown in Fig. 3, whereas the bottom one is perforated and a groove allows the fluid to flow. The bottom plate contained ⌀2 mm holes spaced with a regular distance of 4 mm between each others. The grooves underneath are 2.2 mm wide and regularly spaced at 3.7 mm distance. The plies were individually impregnated with the 200 cSt silicon oil Xiameter PMX 200 (Dow Europe GmbH) for wet experiments. The individual plies were then stacked and gently pressed with a roll such as to evacuate air between them.

The machine was calibrated to correct compliance prior to compression testing in order to enable a precise cavity height measurement. An empty compaction test was performed to check the quality of the compliance correction and to properly set the tool distance before each set of experiments.

2.3. Experimental testing procedure

The experimental testing procedure is based on multiple steps compaction with constant compaction velocity and variable holding times at a given position. The experiment was repeated with the following compaction velocities: 0.1, 0.5, 2.0, 6.0 and 12.0 mm/min, each time with a new textile sample. The compaction velocities were chosen such as to cover a broad range of strain speeds while taking the limits of the mechanical testing machine into account. The test is designed to gain information on the time dependent response of the fibre bed over a range of strains and strain speeds.

The testing procedure consists of twelve compaction steps covering the whole range of fibre volume fractions as summarized in Table 1. The compaction goes on until a defined force is reached before letting the fibre relax at constant strain for a given period of time. The stress is directly obtained by dividing the force with the compaction tool area. The stress differences at each compaction steps are defined as large enough in order to guarantee a minimal tool displacement and a sufficient measurement quality but as small as possible in order to minimize changes in the viscoelastic fibre bed behaviour. This results in a greater relative stress increase at higher fibre volume fractions because of the non-linear fibre behaviour. The first, fourth, seventh and tenth compaction steps are larger steps used as transitions between different regions of fibre volume fractions and are not considered in the evaluation of the model parameters, but are used to verify that the model remains valid at larger strains. The holding time is reduced at lower fibre volume fractions to minimize the total experiment duration.

The fibre bed response is commonly described through its fibre volume fraction v_f rather than its strain. The fibre volume fraction is obtained with Eq. (1), where N is the number of layers, A_w the areal weight of the fabric, ρ the density of the fabric and h the cavity height, which is measured as the cross-head displacement corrected with machine compliance. The strain is directly related to the cavity height with Eq. (2) where the strain ϵ is defined as positive with closing tool distance.

$$v_f = \frac{NA_w}{\rho h} \tag{1}$$

$$\epsilon = \frac{h_0 - h}{h_0} \tag{2}$$

Thereby, h_0 is the initial tool separation distance corresponding to the stack thickness in uncompressed state. These two equations can be combined to relate fibre volume fraction and strain:

$$v_f = \frac{NA_w}{\rho h_0(1-\epsilon)} \tag{3}$$

2.4. Model approach

A Finite Difference Method (FDM) is adopted to obtain the response of the Maxwell model, which can be assumed linear over sufficiently small intervals. The model response of a Maxwell model is the sum of the stresses of the individual branches. For the present case with three viscoelastic branches it reads:

$$\sigma = \sigma_0 + \sum_{i=1}^{i=3} \sigma_i \tag{4}$$

where σ is the stress, the superscript 0 denotes the elastic branch and the superscripts from 1 to 3 the viscoelastic branches. The stress response of the elastic branch is given by Eq. (5). For the branches with a spring and a damper in series the viscoelastic behaviour is strain-rate dependent [26] and the stress response is described with the constitutive Eq. (6).

$$\sigma_0 = E_0(\epsilon)\epsilon \tag{5}$$

$$\frac{\partial \epsilon}{\partial t} = \frac{1}{E_i}\frac{\partial \sigma_i}{\partial t} + \frac{\sigma_i}{\eta_i(\dot{\epsilon})} \tag{6}$$

$$\tau(\dot{\epsilon}) = \frac{\eta_i(\dot{\epsilon})}{E_i} \tag{7}$$

In these equations ϵ is the overall strain and σ the stress. The superscript 0 denotes the elastic branch and the superscripts from 1 to 3 the viscoelastic branches. $E(\epsilon)$ is the strain dependent Young's modulus, $\eta_i(\dot{\epsilon})$ the strain-rate dependent viscosity of the dashpot elements and $\tau_i(\dot{\epsilon})$ their corresponding relaxation time. With the FDM approach the derivatives are transformed into finite differences δ and the viscoelastic branches are linearized. This implies that the parameters of these branches are constant over δt and the strain rate as well. Relating the dashpot viscosity with the relaxation time as expressed in Eq. (7) into (6) yields:

$$\sigma_i(t+\delta t) = \sigma_i(t) + E_i\delta\epsilon_i - \frac{\sigma_i}{\tau_i(\dot{\epsilon})}\delta t \tag{8}$$

This equation can be solved if the initial conditions are known. We assume that the fibre bed is completely relaxed at the end of each step, contiguous to the start of the next compaction. The stress in each viscoelastic branch is therefore zero as initial conditions. Bringing together Eqs. (4), (5) and (8) enables to numerically solve the Maxwell model with:

$$\sigma(t+\Delta t) = E_0(\epsilon)\epsilon + \sum_{i=1}^{i=3}\left[\sigma_i(t) + E_i\Delta\epsilon_i - \frac{\sigma_i}{\tau_i(\dot{\epsilon})}\delta t\right] \tag{9}$$

This approach provides the stress response as a function of time if the model parameters are already known. However, there is no direct way to extract these parameters with known stress response. The measured stress response for a given strain input is therefore compared

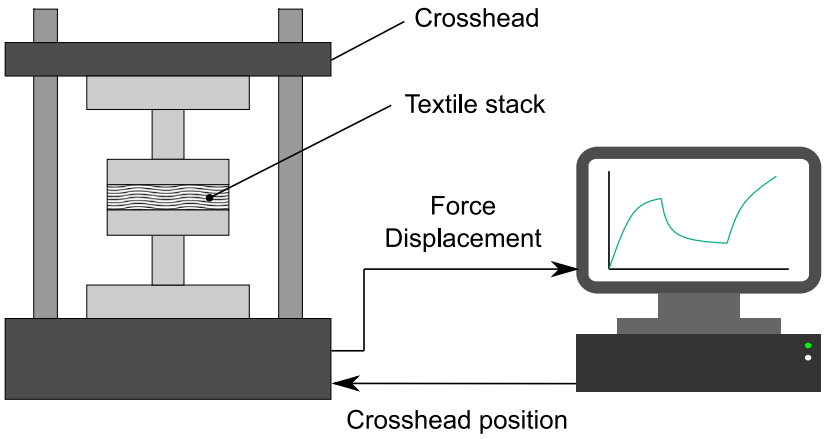

Fig. 3. Setup of the compaction test.

to the stress response obtained with the FDM method and a given set of parameters. The parameters are then optimized with a Simplex algorithm [27] such that the FDM model response corresponds to the measurements. The algorithm is implemented in a three dimensional manner, meaning that three parameters can be optimized at once while the others are fixed. At each iteration, the model response is calculated with the FDM method and the current set of parameters. The sum of the square differences (SSQ) between the FDM model response $\sigma_{FDM}(t)$ and the measurements $\sigma(t)$ is evaluated with Eq. (10). Based on that, the algorithm defines a new set of model parameters such as to minimize the SSQ. The iteration goes on until convergences is observed, at which point the parameters are returned as solution.

$$SSQ = \sum_{t_{start}}^{t_{end}} \left[\left(\sigma_{FDM}(t) - \sigma(t) \right)^2 \right] \tag{10}$$

The sampling rate was set to make a measurement each 0.25s or if the tool displacement exceeded 10 μm. As this time scale is one order of magnitude lower than the effects taking place in the branch with the fastest relaxation time (around 2s), the time interval is sufficiently small for the behaviour to be well approximated as linear. The approach to determine the parameters of the Maxwell model is very similar to that proposed by Danzi [18]. In the procedure that we have defined, no more than three parameters will be determined at once, meaning that the three dimensional optimization algorithm described above is sufficient. The properties found with the fitting algorithm at each of the compaction steps are associated with the fibre volume fraction at the beginning of the holding step.

The model parameters extraction can be separated in three stages. During the first step the strain dependent compression modulus of the elastic branch $E_0(v_f)$ is extracted. Then, the Young's moduli $E_i(v_f)$ of the viscoelastic branches are determined at the reference strain speed. Finally, the strain-rate dependent relaxation times $\tau_i(\dot{\epsilon})$ are extracted. During this procedure the large compaction steps (N° 1,4,7 and 10, see Table 1) are not considered. Note that the Young's moduli are expressed as function of the fibre volume fraction in the following and can easily be transformed as a function of the strain using Eq. (2).

Stage 1: Definition of the compression modulus.

The elastic branch of the Maxwell model is responsible for the quasi-static response of the fibre bed. The stress and strain values at the end of the different steps form the quasi-static compaction curve because it is assumed that the fibre-bed is completely relaxed at the end of each compaction step. This curve takes an exponential form as suggested by Robitaille and Gauvin [28] and we fit it to Eq. (11). In this equation, A and B are fitting parameters while v_{f0} is the initial fibre volume fraction. The strain is calculated based on the cavity height h_0 which we measured at the preload of 5N, see Table 1. Fitting of the quasi-static datapoints to Eq. (11) allows to extract the Young's Modulus of the elastic branch $E_0(v_f)$. Due to measurements errors it can happen that a force is recorded at the measured v_{f0}, leading to a divide by zero in Eq. (11), therefore v_{f0} is fitted as well rather than measured.

$$E_0(v_f) = \frac{A \cdot e^{B \cdot v_f}}{\left| \frac{v_{f0}}{v_f} - 1 \right|} \tag{11}$$

Stage 2: Definition of the Young's moduli of the viscoelastic branches.

The stiffness parameters E_i of the three viscoelastic branches are extracted with the optimization algorithm explained earlier at each compaction step of the reference speed, which we arbitrarily set to 2 mm/s. Thereby we consider that these stiffnesses are constant over each compaction step. Meaningful guessed values are used for the relaxation times: 2, 20 and 200 s which were found to provide good fits. Using the model parameters derived in Stage 1 for the Young's modulus $E_0(v_f)$ comes along with its fitting error. As a result, the measured stress might be incorrectly parted into elastic and viscoelastic stress, which will not tend towards zero for quasi-static states at the beginning and end of the compaction steps. Incorrect determination of the viscoelastic stress will perturb the optimization algorithm and cause improper parameter extraction. For this reason, we define a measured Young's modulus for each compaction step by fitting the quasi-static values at the beginning and the end of the current step to Eq. (11), where the fitted value of v_{f0} obtained in stage one is used. This stiffness is not constant but a function of the measured fibre volume fraction. Note that the measured Young's modulus is only used for parameter extraction and will not be part of the model.

Fig. 4 represents the strain input imposed to the fibre bed and the corresponding measured stress response. The elastic stress response obtained with the Maxwell model on the basis of the measured and modelled Young's modulus are displayed as well. The measured stiffness yields a correct quasi-static stress response and allows a proper extraction of the measured elastic stress response. The optimization algorithm will fit the stiffness parameters to the viscoelastic response, which is the difference between the measured stress and the elastic response. The fitting procedure yields a set of stiffness parameters E_i for each compaction step. These display an exponential dependence on the fibre volume fraction and are fitted to a function of the form $A \cdot e^{B \cdot v_f}$. The parameter set for the second stage is summarized in Table Table 2.

Stage 3: Definition of the relaxation times.

The third stage aims at describing the variation of the relaxation times as a function of the strain speed. The FDM model uses the same compaction modulus E_0 for the same reasons, as well as the set of stiffness parameters E_i obtained in Stage 2 for the viscoelastic branches, still considered as constant over the individual compaction steps. During parameter extraction, the relaxation times are fitted to the measurements for each compaction step at the different compaction speeds with the optimization algorithm. The relaxation times are assumed constant within a compaction step. The fitted variables are then

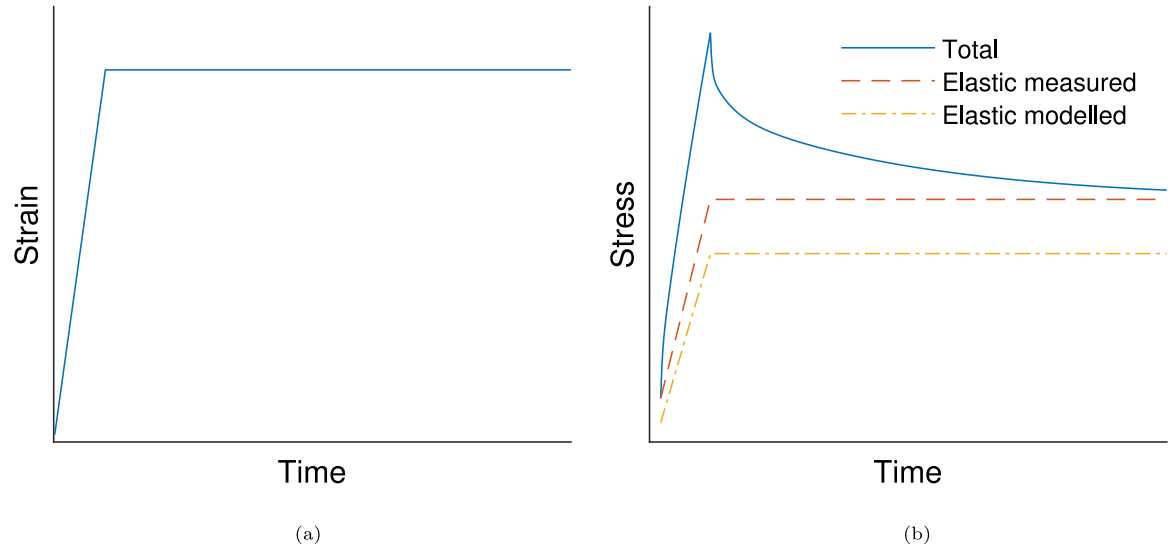

Fig. 4. Fig. 4(a): Representation of the strain curve imposed to the fibre bed. Fig. 4(b): Representation of the corresponding measured stress response along with the elastic stress modelled with the FDM method based on different Young's moduli. The label "measured" indicates that the measured stiffness has been used while the label "modelled" is linked to the stiffness derived in stage one.

associated with the measured average strain speed at each step, which corresponds to the strain difference from the start of compaction to the start of relaxation over the elapsed time. The relaxation times with respect to the strain speed are finally fitted to a function of the form $A \cdot \dot{\epsilon}^{-B}$, which is found to provide a better fit than the function $A \cdot e^{B \cdot \dot{\epsilon}}$ proposed by Danzi [18]. The parameter set for the second stage is summarized in Table Table 3.

2.5. Model accuracy

To quantify the accuracy of the model, the stress response of the fibre bed is calculated for each compaction step based on the measured strain with the resulting model and compared to the measured stress response. At the beginning and towards the end of a compaction step, the difference corresponds to the modelling error of the elastic branch since the viscoelastic response is negligible. However, at the peak stress the viscoelastic response is the highest and we expect the modelling error to overall reach its maximum at this point. For this reason, the model accuracy is measured at the peak stress.

The total model error is the sum of the errors emanating from the elastic and viscoelastic branches and they can add up but also subtract from each other. It is desirable to know the extent of their respective contribution to the total model error, which cannot yet be directly read from the measurements. For this reason, the measured stress response is parted into an elastic and viscoelastic part using the same method presented in the second stage based on the measured Young's modulus. At the peak measured stress, it reads:

$$\sigma^{\max}_{\text{meas.}}(\epsilon, \dot{\epsilon}) = \sigma^{\max}_{\text{E,meas.}}(\epsilon) + \sigma^{\max}_{\text{VE,meas.}}(\dot{\epsilon}) \tag{12}$$

where the subscript meas. denotes the measured stress, max that the property is measured at the peak stress, E the elastic and VE the viscoelastic stress. The modelled peak stress obtained with the FDM method is easily parted into elastic and viscoelastic parts and it can be written as:

$$\sigma^{\max}_{\text{model}}(\epsilon, \dot{\epsilon}) = \sigma^{\max}_{\text{E,model}}(\epsilon) + \sigma^{\max}_{\text{VE,model}}(\dot{\epsilon}) \tag{13}$$

The total relative modelling error is defined in Eq. (14). The measured relative elastic error is defined in Eq. (15) as the difference between the measured and modelled elastic stress at the peak stress divided by the measured peak stress. The measured relative viscoelastic error is defined in a similar way in Eq. (16).

Table 2
Parameter set for the second stage.

$E_0(\nu_f)$	Approximated at each step
E^i_1, E^i_2, E^i_3	Fitting variable
$\tau_1 = 2$, $\tau_2 = 20$, $\tau_3 = 200$	Fixed parameters

Table 3
Parameter set for the third stage.

$E_0(\nu_f)$	Approximated at each step
E^i_1, E^i_2, E^i_3	Derived in Stage 2
τ_1, τ_2, τ_3	Fitting variables

$$\text{Error} = \frac{|\sigma^{\max}_{\text{meas.}}(\epsilon, \dot{\epsilon}) - \sigma^{\max}_{\text{model}}(\epsilon, \dot{\epsilon})|}{\sigma^{\max}_{\text{meas.}}(\epsilon, \dot{\epsilon})} \tag{14}$$

$$\text{Error}_{\text{E}} = \frac{|\sigma^{\max}_{\text{E,meas.}}(\epsilon) - \sigma^{\max}_{\text{E,model}}(\epsilon)|}{\sigma^{\max}_{\text{meas.}}(\epsilon, \dot{\epsilon})} \tag{15}$$

$$\text{Error}_{\text{VE}} = \frac{|\sigma^{\max}_{\text{VE,meas.}}(\dot{\epsilon}) - \sigma^{\max}_{\text{VE,model}}(\dot{\epsilon})|}{\sigma^{\max}_{\text{meas.}}(\epsilon, \dot{\epsilon})} \tag{16}$$

3. Results

3.1. Materials

The measured material properties are reported in Table 4. The densities of the fabrics are in the expected range for carbon and glass. The small deviations can arise due to different fibre types, sizing or experimental measurement errors. The textile architecture influences the fibre volume fraction and thus the number of layers required to reach a certain thickness in uncompressed state. The thickness of the glass mat is above the target value, but we do not expect it to have any impact on the measured strain or outcome.

3.2. Definition of model parameters

In the following, the analysis and illustrations describes the results obtained with the carbon plain weave in dry condition if not explicitly specified otherwise. These results are representative of the behaviour

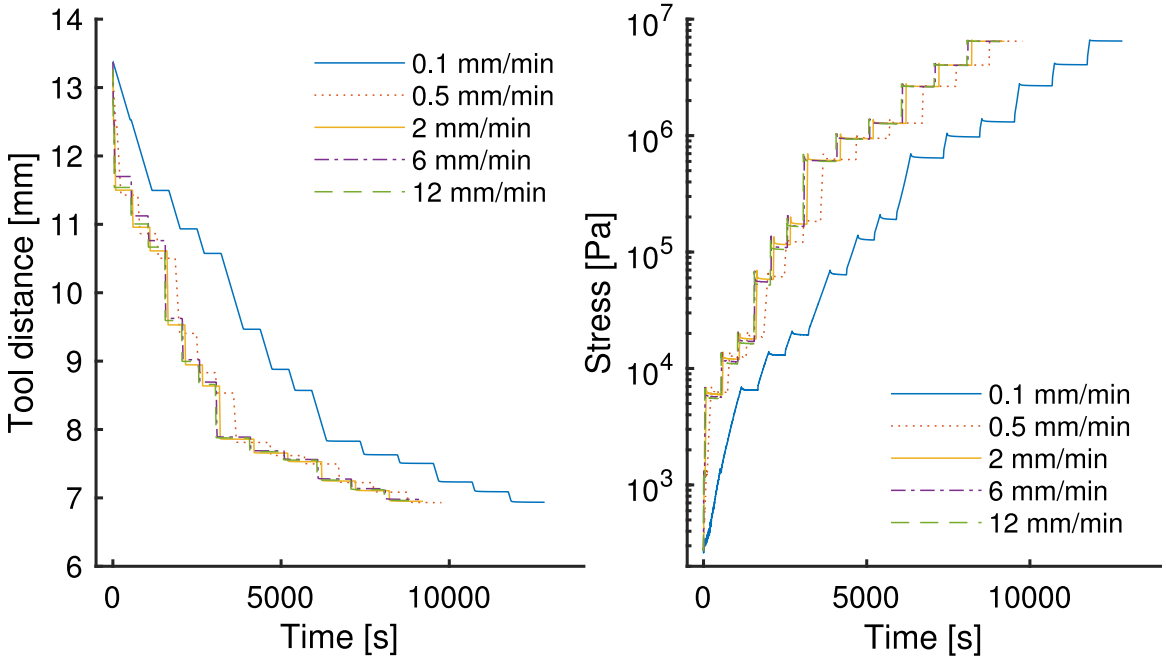

(a) (b)

Fig. 5. 5(a): Tool distance as a function of time for the multiple compaction steps at different strain rates for the carbon plain weave in dry condition. 5(b) Corresponding measured stress as a function of time.

Table 4
Material properties of the different fabrics and measured initial sample height.

Fabric	Areal weight [$\frac{g}{m^2}$]	Density [$\frac{kg}{m^3}$]	Number of layers	Sample height [mm]
Glass mat	571	2400	14	17.1
Glass quasi-UD	931	2524	16	13.8
Carbon plain weave	203	1754	45	13.3
Carbon biaxial	571	1711	14	13.9

observed with the other textiles in both dry and wet conditions. Different or noticeable behaviour of the other fabrics are described when relevant for the analysis.

Fig. 5 shows the tool distance and resulting stress value obtained for a multiple steps compaction test, which is the basis of the following analysis. Even though the initial sample thickness is similar for all the fabrics, we obtain varying final sample thicknesses because of the different textile behaviour. Still, the strain profile is comparable each time and we do not expect it to have any effect on the analysis.

Stage 1: Fig. 6 shows the quasi-static stress response of the five multiple steps compaction experiments performed at different strain rates, and the resulting fitted curve. We obtain an overall good fit quality over the entire data set which spans over the whole range of fibre volume fractions. Note that the measured value typically spans over several order of magnitudes due to the exponential behaviour of the fibre beds and the measurements covering the whole range of fibre volume fractions. The fitting of the Young's moduli is performed in a logarithmic scale because it ranges over three order of magnitudes.

The coefficients of determination R^2 of the fits for the different experiments are listed in Table 5. We obtain an excellent fit quality, comparable for all the experiments. Yet, we also observe a relatively elevated scatter of the measurements which is acceptable because fibre beds are known to display such a behaviour. The fit quality is comparable in dry and wet conditions. The fibre beds display a lower stiffness in wet conditions, as observed by several authors [12]. Lubricated fibres can slide past each other and rearrange themselves more easily due to a reduced friction. Table 6 summarizes the fitted parameters

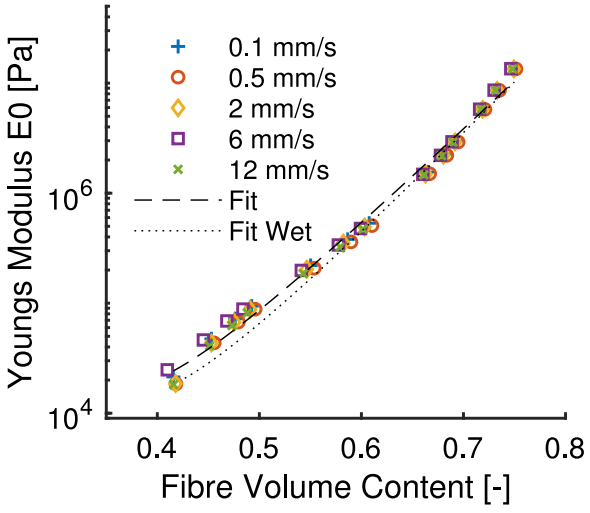

Fig. 6. Quasi-static data points of the Young's modulus E_0 in function of the fibre volume content obtained with different compaction speeds and resulting fitting curve for the carbon plain weave in dry condition. The fitting curve of the carbon plain weave obtained in wet conditions is displayed along for comparison.

of Eq. (11) obtained for the different tests. The stiffening parameter B is responsible for the shape of the exponential curve, the parameter A is a simple multiplication factor and v_{f0} corresponds to the fibre volume fraction in uncompressed state.

The stiffening parameter remains rather constant for a same material independently of its state. However, the multiplication factor decreases in wet state, indicating that the quasi-static stress response is smaller at equal fibre volume fraction. The fitted uncompressed fibre volume fractions in dry and wet states are very close to each other, except for the quasi-UD weave. The v_{f0} obtained are generally smaller than the fibre volume fraction measured at the preload of 5N, which is an expected behaviour considering the very low stiffness of fibre beds

Table 5
Resulting fit quality of the different experiments.

Material	State	R^2
Glass mat	Dry	0.992
Glass mat	Wet	0.996
Glass quasi-UD	Dry	0.988
Glass quasi-UD	Wet	0.991
Carbon biaxial	Dry	0.996
Carbon biaxial	Wet	0.994
Carbon plain weave	Dry	0.993
Carbon plain weave	Wet	0.992

Table 6
Resulting model parameters for the compression modulus E_0.

Material	State	A	B	ν_{f0}
Glass mat	Dry	94.64	16.42	0.144
Glass mat	Wet	70.17	16.98	0.153
Glass quasi-UD	Dry	0.12	22.93	0.276
Glass quasi-UD	Wet	0.03	24.22	0.414
Carbon biaxial	Dry	1.14	19.91	0.279
Carbon biaxial	Wet	0.68	20.66	0.262
Carbon plain weave	Dry	0.71	21.23	0.333
Carbon plain weave	Wet	0.26	22.49	0.348

close to their uncompressed states. This trend is not observed for the quasi-UD glass weave in dry conditions and we impute this behaviour to a poorer fit, also observable in Table 5. The values obtained at the first stage otherwise reflect an expected behaviour.

When comparing the different materials we observe that the range of stiffnesses is rather similar and from 10^4 to 10^7 Pa in dry conditions. The carbon plain weave has a higher stiffness at low fibre volume fractions ($2.2{\cdot}10^4$ Pa), probably because the weaving contributes to a higher initial number of contact points between bundles. The range of fibre volume fractions is changing depending on the material and degree of fibre alignment. The quasi-UD weave and the carbon biaxial fibres with straight fibres reach the highest fibre volume fraction at maximal load with 0.78, the carbon weave slightly less with 0.75, the glass dry fibres only 0.67 since the fibres are neither aligned nor organized. The fibre volume fraction at the preload is also significantly lower for the glass mat with a fibre volume fraction of 0.2 against 0.38 to 0.46 for the other materials.

Stage 2: Fig. 7(a) shows an average result of the stiffness parameter extraction procedure, for which the modelled stress response is fitted to the measured one. We observe an overall very good fit quality with higher deviation in the mid-term holding step. The long-term stress response error is rather low and corresponds to the remaining stress in the viscoelastic branches, validating the quasi-static assumption at the end of the compaction steps. We also note that the fit quality slightly decreases at very high fibre volume fraction, yet remains largely acceptable. The stress response of the individual viscoelastic branches of the Maxwell model for the fitted curve shown in Fig. 7(a) is displayed in Fig. 7(b).

At the end of the stiffness parameter extraction, the set of relaxation times in function of the fibre volume fraction is fitted for each of the parameter E_1, E_2 and E_3 as shown in Fig. 8(a) on a logarithmic scale. The quality of the fit is very good for all the three branches, whose Young's moduli once again span over three order of magnitudes. For comparison, the same fit is displayed for the carbon plain weave in wet condition in Fig. 8(b). One can see that the two figures display a strikingly similar behaviour. The difference of values in dry of wet conditions are hardly noticeable because of the logarithmic scale. The stiffness is decreasing from the first to the third branch, however the amplitude of their response is comparable because of the increasing relaxation time as shown in Fig. 7(b).

Table 7 summarizes the result of the fitting procedure for all the samples, where similar fitting results are obtained. We observe that the

Table 7
Resulting fit quality of the quasi-static compaction curve.

Sample	State	R^2 value		
		E_1	E_2	E_3
Glass mat	Dry	0.994	0.997	0.995
Glass mat	Wet	0.996	0.996	0.996
Glass quasi-UD	Dry	0.996	0.985	0.977
Glass quasi-UD	Wet	0.995	0.987	0.978
Carbon biaxial	Dry	0.990	0.995	0.992
Carbon biaxial	Wet	0.998	0.997	0.994
Carbon plain weave	Dry	0.999	0.992	0.977
Carbon plain weave	Wet	0.999	0.997	0.982

Table 8
Resulting model parameters for the Young's moduli E_i.

Material	State	Branch	A	B
Glass mat	Dry	E_1	99.1	23.9
		E_2	210	20.7
		E_3	17.1	24.0
	Wet	E_1	244	22.0
		E_2	271	20.1
		E_3	28.1	23.1
Glass quasi-UD	Dry	E_1	$6.01{\cdot}10^{-1}$	26.2
		E_2	$7.82{\cdot}10^{-3}$	29.7
		E_3	$3.65{\cdot}10^{-4}$	33.4
	Wet	E_1	$1.22{\cdot}10^{-1}$	28.1
		E_2	$1.36{\cdot}10^{-3}$	31.8
		E_3	$8.03{\cdot}10^{-5}$	35.2
Carbon biaxial	Dry	E_1	6.51	23.0
		E_2	1.57	23.2
		E_3	$6.53{\cdot}10^{-2}$	27.0
	Wet	E_1	48.7	20.5
		E_2	1.42	23.2
		E_3	$8.54{\cdot}10^{-2}$	26.4
Carbon plain weave	Dry	E_1	3.20	23.8
		E_2	$6.63{\cdot}10^{-2}$	26.2
		E_3	$4.20{\cdot}10^{-3}$	29.4
	Wet	E_1	$2.22{\cdot}10^{-1}$	29.3
		E_2	$1.04{\cdot}10^{-1}$	25.8
		E_3	$6.99{\cdot}10^{-4}$	32.1

fit is usually better suited to the fibre beds in wet conditions. Such a behaviour might be explained by the fact that fibres gliding past each other can be modelled with a viscoelastic model, which is however less suited when the fibres are sliding because it is a friction-based mechanism.

Table 8 displays the parameters resulting from the fitting of the individual viscoelastic branches for the different tests. We observe that the stiffening factor B is rather similar in dry and wet conditions as expected. The different materials exhibits similar viscoelastic branches stiffness behaviour over the range of measured fibre volume fraction. In uncompressed state, the dry glass mat has almost equivalent stiffnesses E_1 and E_2 whereas the first is about one order of magnitude larger than the latter in other textiles.

Stage 3: Fig. 9 shows a typical result of the relaxation time extraction procedure, for which the modelled stress response is fitted to the measured one. The quality of the fit is improved when compared to stage 2 since all of the parameters have been extracted. The fit quality at other compaction speeds is of comparable quality. Figs. 9(a) and 9(b) compare the fit for the carbon plain weave in dry and wet conditions, one can see similar fit qualities. These two Figures also allows to observe the change of behaviour in the textile response when in wet condition, one can clearly see that the amplitude of the relaxation is more pronounced when wet.

The obtained relaxation times with corresponding measured compaction speeds have been fitted for the different viscoelastic branches as shown in Fig. 10, which displays both the dry and the wet case. In the dry case, we obtain a fit quality which is decreasing from the first

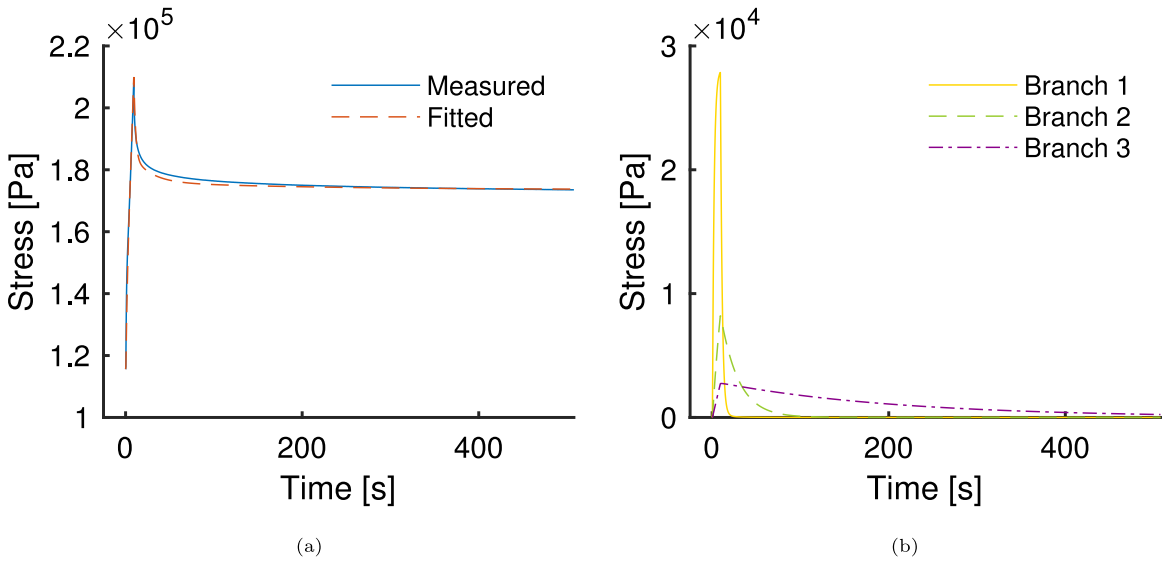

Fig. 7. Fig. 7(a) displays the measured fibre bed stress response in function of the time for the sixth compaction step at reference speed for the carbon plain weave in dry condition, along with the result of the fitting procedure. Fig. 7(b) displays the stress response of the individual viscoelastic branches of the Maxwell model.

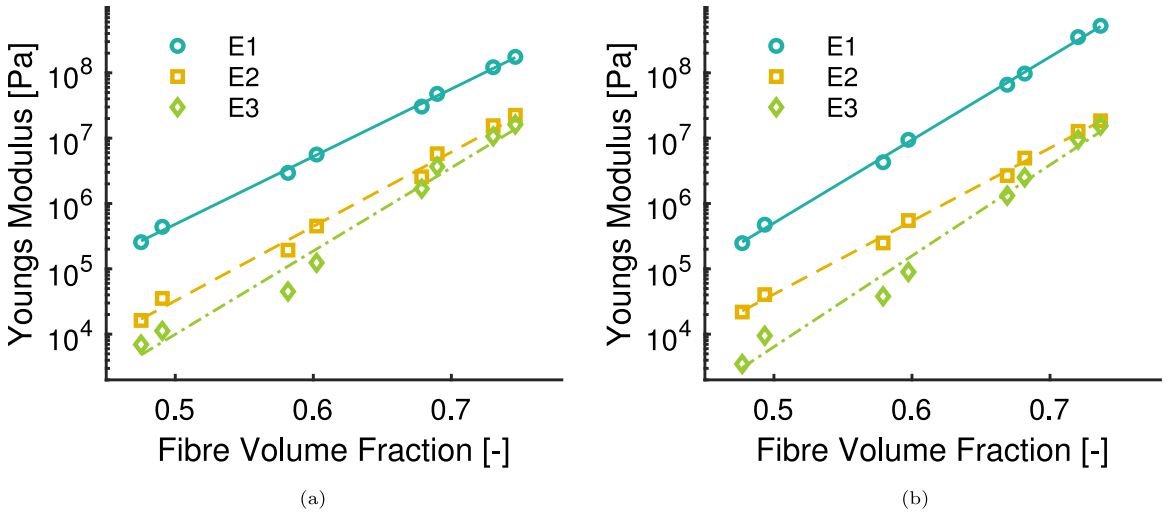

Fig. 8. Stiffness value of the different viscoelastic branches as a function of the fibre volume fraction for the reference compaction speed of the carbon plain weave in dry condition in Fig. 8(a) and in wet condition in Fig. 8(b).

to the third branch. While for the first branch the fit is very good, it is fair for the second and poor for the third. In any cases, the mean relative error between the data points and the fit is 7.7% so that the accuracy remains sufficient. The relaxation time for the third branch seems to depend linearly on the strain speed rather than exponentially. The reader will notice that although five different compaction velocities have been prescribed, the measured strain rates are rather dispersed. This is due to the actuation error of the machine, which tend to increase at more elevated compaction velocities. We observe that the fit quality decreases in wet conditions, but overall the same considerations apply.

Table 9 displays the R^2 values of the three branches for the different experiments. We globally observe the same trends and fit quality in all the experiments. The carbon plain weave displays a noticeable behaviour in the fitting of E_3 since the other fabrics have much better fit qualities. Table 10 displays the parameters resulting from the fitting of the relaxation times for the different tests. We observe similar trends and no particular differences between the relaxation times of the different materials.

Modelling Error: The quality of the model is appreciated by modelling the stress as a function of time for the different compaction steps based on the measured strains before weighting it against the measured stress curves. Fig. 11 shows an example highlighting the difference between the modelled and measured stress, in this case for a large compaction step. Note that the difference between the curves towards the end of the compaction step is entirely due to fitting inaccuracies of E_0, which can be an important source of discrepancy between measurements and predictions.

Table 9
Resulting fit quality of the quasi-static compaction curve.

Sample	State	R^2 value		
		τ_1	τ_2	τ_3
Glass mat	Dry	0.831	0.706	0.420
Glass mat	Wet	0.860	0.803	0.766
Glass quasi-UD	Dry	0.914	0.608	0.466
Glass quasi-UD	Wet	0.905	0.582	0.355
Carbon biaxial	Dry	0.962	0.731	0.315
Carbon biaxial	Wet	0.905	0.750	0.304
Carbon plain weave	Dry	0.966	0.929	0.059
Carbon plain weave	Wet	0.775	0.963	0.854

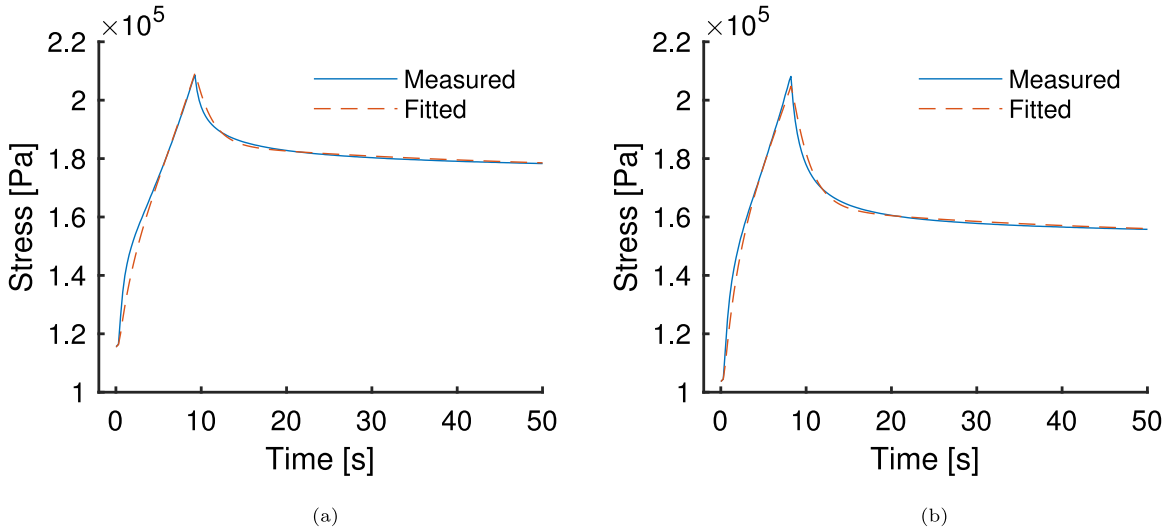

Fig. 9. Measured fibre bed stress response as a function of the time for the sixth compaction step of the carbon plain weave in dry condition in Fig. 9(a) and in wet condition in Fig. 9(b) at reference speed, along with the result of the fitting procedure during the relaxation time parameters extraction.

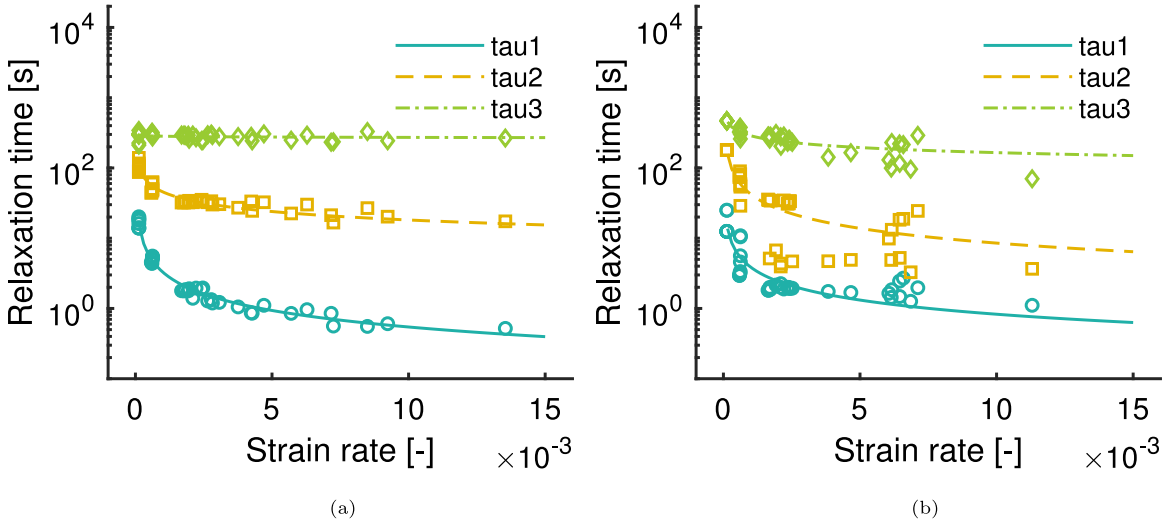

Fig. 10. Relaxation times of the different viscoelastic branches in function of the compaction speed for the carbon plain weave in dry condition in Fig. 10(a) and wet condition in Fig. 10(b).

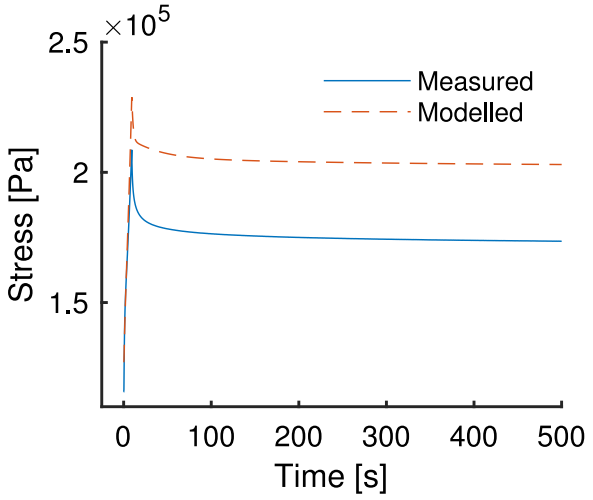

Fig. 11. Measured and modelled stress in function of the time for the sixth compaction step at reference speed for the carbon plain weave in dry condition.

Fig. 12 displays the modelling error averaged over the different compaction speeds in Fig. 12(a) and the compaction steps in Fig. 12(b). We observe little variation of the model accuracy over the whole range of the compaction speeds. As the viscoelastic response becomes larger at more elevated strain speeds, its contribution to the modelling error raises as well. When averaged over the different compaction steps, we observe that the modelling error has important discrepancies. This behaviour can be explained on one hand by the different fit qualities which can change from location to location. On the other hand, the total error is the sum of the errors of the elastic and viscoelastic branches, which can either add up or cancel each other.

In Fig. 12(b) the results for the large compaction steps – the first, fourth, seventh and tenth step – do not stand out, validating the model even at larger strains. Overall, the mean modelling error amounts to 12.98%, which is very accurate considering that fibre beds displays large discrepancies in their behaviour.

Analytical models as presented in [10,18,20] assume a perfectly constant strain during relaxation, and many present constitutive equations based on a generalized linear Maxwell model where the stiffness E_0 is assumed constant over a small compaction step. As we consider small variations in strain during relaxation, assuming a constant elastic

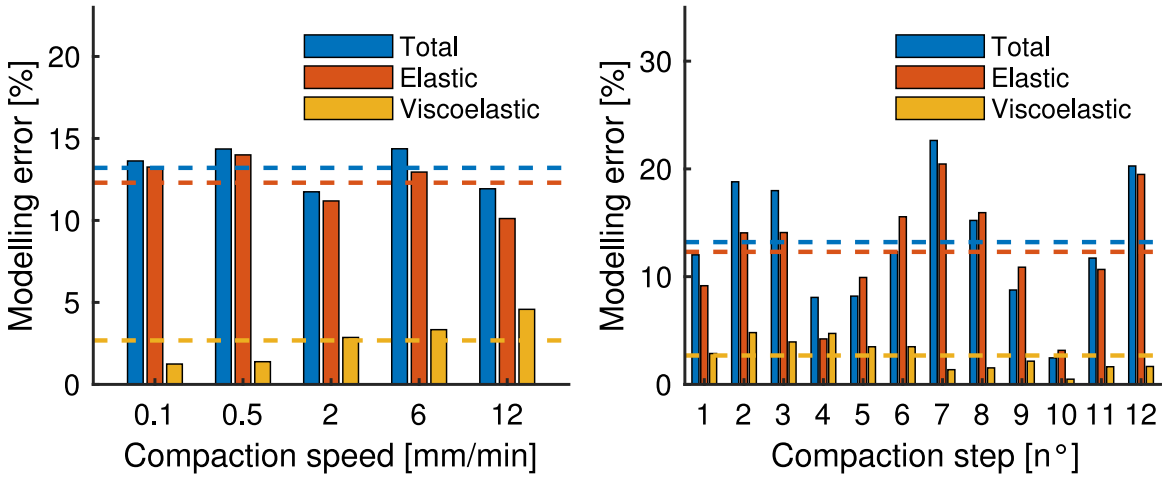

Fig. 12. Fig. 12(a) shows the mean modelling error over different compaction speeds for the carbon plain weave in dry condition and Fig. 12(b). The dashed line is the overall mean modelling error.

Table 10
Resulting model parameters for the relaxation times τ_i.

Material	State	Branch	A	B
Glass mat	Wet	τ_1	$2.04 \cdot 10^{-2}$	0.73
		τ_2	1.61	0.46
		τ_3	178	$6.26 \cdot 10^{-2}$
	Wet	τ_1	$6.79 \cdot 10^{-2}$	0.59
		τ_2	1.37	0.50
		τ_3	120	0.13
Glass quasi-UD	Wet	τ_1	$1.46 \cdot 10^{-2}$	0.78
		τ_2	5.34	0.30
		τ_3	188	$5.81 \cdot 10^{-2}$
	Wet	τ_1	$1.16 \cdot 10^{-2}$	0.81
		τ_2	4.35	0.32
		τ_3	173	$6.43 \cdot 10^{-2}$
Carbon biaxial	Wet	τ_1	$1.73 \cdot 10^{-2}$	0.77
		τ_2	3.18	0.38
		τ_3	204	$4.72 \cdot 10^{-2}$
	Wet	τ_1	$2.19 \cdot 10^{-2}$	0.71
		τ_2	1.46	0.49
		τ_3	149	$8.24 \cdot 10^{-2}$
Carbon plain weave	Wet	τ_1	$1.49 \cdot 10^{-2}$	0.78
		τ_2	2.88	0.40
		τ_3	252	$1.71 \cdot 10^{-2}$
	Wet	τ_1	$3.79 \cdot 10^{-2}$	0.67
		τ_2	0.34	0.70
		τ_3	54.7	0.24

stiffness E_0 is not reasonable because of its exponential behaviour. The numerical method presented thus considers the measured strain and introduces a variable stiffness $E_0(\nu_f)$ to correctly model the elastic stress. This results in a better parameter extraction as the measured stress is more accurately parted into elastic and viscoelastic stress. The stiffnesses of the viscoelastic branches are yet still assumed constant during the parameter extraction and the compaction steps are kept as small as possible for this reason. The impact of this assumption is thought to be rather small but should still be quantified in future work.

Table 11 displays the mean modelling error of the different experiments. The accuracy of the viscoelastic model is globally lower when applied to wet fibre beds. Albeit this decreasing accuracy, the modelling errors are deemed to remain fully acceptable. We suppose that the variations of the mean modelling errors between the different materials either in dry or wet conditions are mainly due to statistical effects. It is very interesting to note that while for some fabrics the main source of modelling error comes from the elastic branch, for others it is the viscoelastic ones. One should also keep in mind that as the viscoelastic stress response becomes larger, the modelling error repartition will shift towards the viscoelastic part according to Eqs. (15) and (16).

Table 11
Resulting modelling accuracy of the different samples.

Material	State	Mean modelling error [%]		
		Total	Elastic	Viscoelastic
Glass mat	Dry	16.38	8.57	11.58
Glass mat	Wet	13.32	6.64	11.52
Glass quasi-UD	Dry	18.38	13.13	5.79
Glass quasi-UD	Wet	13.82	11.37	5.40
Carbon biaxial	Dry	12.38	7.77	7.37
Carbon biaxial	Wet	20.19	8.94	14.12
Carbon plain weave	Dry	12.98	12.30	2.31
Carbon plain weave	Wet	18.68	10.51	14.10

3.3. Influence of strain deviations

We noticed significant differences between the prescribed and the measured strains, especially at higher loads. This behaviour is thought to be primarily caused by a combination of machine deflection and actuation error. Machine deflection can be well observed in Fig. 13, where one can see the measured strain significantly deviating from the prescribed strain during relaxation. Regarding the actuation error, we observe that the measured average strain speed considerably differs from the prescribed one at elevated loads and strain speeds. This indicates that the testing machine is getting closer to its limits. An analytical approach is mostly adopted in the literature, in which the assumed ideal strain profile is based on the strain profile prescribed to the machine, yet we note high discrepancies between the prescribed and measured strain profiles. Although analytical methods could be based on the measured average strain speed instead of the prescribed one, this is not a standard practice. We also observe that the strain speed is not perfectly constant during compaction, which is another consequence of actuation error that is not considered in analytical methods.

To investigate the effects of strain deviations on the results, the model parameters at reference were extracted with the assumed strain as input to the FDM model at each step. The assumed strain profile consists of a compaction at constant strain rate until the strain value corresponding to the measured fibre volume fraction at the end of relaxation is reached. The strain rate is set at the measured strain

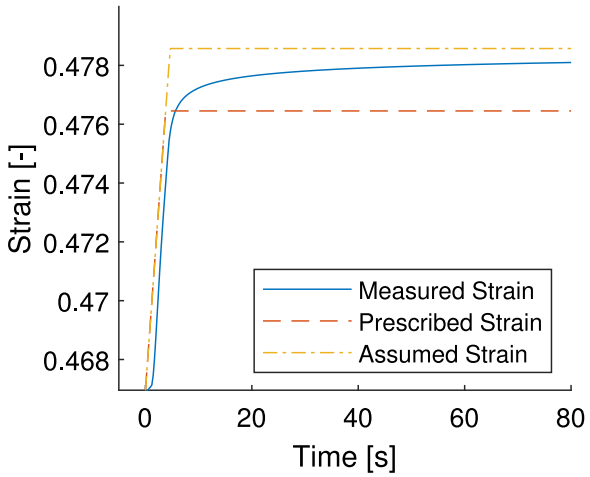

Fig. 13. Strain as a function of time during a compaction step, as prescribed to the testing machine, as assumed for the analytical model and as measured for the twelfth compaction step at reference speed for the carbon plain weave in dry condition.

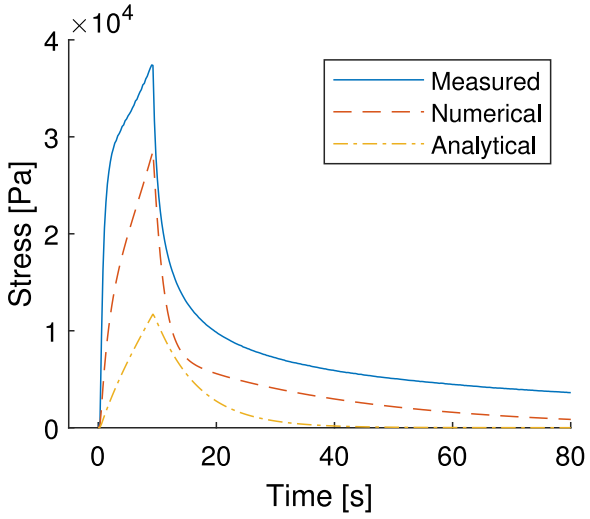

Fig. 14. Measured viscoelastic stress along with the stress modelled based on the parameters extracted with the numerical and analytical methods for the sixth compaction step at reference speed for the carbon plain weave in dry condition.

rate. Then, a constant strain is assumed until the end of the relaxation step. An example of the assumed strain profile is shown in Fig. 13, as compared to the prescribed strain and the measured strain. The stress response was modelled based on the measured strain and the extracted model parameters and compared to the measured stress. The modelling error was calculated with the same procedure as mentioned earlier. The elastic parameters are not affected by actuation error and we thus consider the viscoelastic modelling error only.

Fig. 14 displays an example of measured viscoelastic stress along with two stress curves modelled based on the measured strain profile and parameters extracted either with the measured or assumed strain profile. As one can see, the difference between the two stress curves is consequent and the analytical method yields far less precise results. This highlights the necessity to consider the effects of strain deviations during parameter extraction to accurately describe the viscoelastic behaviour of textiles. Using an assumed ideal strain will otherwise result in erroneous model parameter definition and incorrect stress modelling of the fibre bed.

In Fig. 15 we compare the viscoelastic modelling error obtained numerically (measured strain) and analytically (assumed strain). The

Table 12
Resulting modelling accuracy of the different samples.

Material	State	Mean Viscoelastic modelling error [%]	
		Numerical	Analytical
Glass mat	Dry	11.58	26.45
Glass mat	Wet	11.52	22.30
Glass quasi-UD	Dry	5.79	7.80
Glass quasi-UD	Wet	5.40	10.85
Carbon biaxial	Dry	7.37	16.40
Carbon biaxial	Wet	14.12	19.56
Carbon plain weave	Dry	2.31	8.85
Carbon plain weave	Wet	14.10	14.86

viscoelastic error increases by a factor higher than three if actuation error is not considered. We obtain a significantly greater modelling error with the numerical method even for the firsts compaction steps with low stress levels, which is unexpected. The difference between the numerical and analytical modelling error is rather constant over the range of applied loads and compaction speeds as on can see in Fig. 15(b). Another interesting observation is that the relaxation times are closer to a constant value when extracted with the measured strain profile, as it should be according to the model assumptions. This behaviour is certainly based on the fact that the measured and assumed strain speed can significantly differ from each other. The same analysis was repeated for all the experiments and the results are reported in Table 12, where the same trends are observed for all experiments.

It is known that precise measurement of the tool distance is necessary for accurate compaction tests. The previous findings underly the importance of both correct strain and strain rate measurement. However, the extent of the effects of strain deviations is noteworthy. Hence, more accurate methods should be used in future works such as the one proposed by Sousa and al. [24], which measures both loading and unloading compliance. In addition, one should carefully consider the limits of the testing equipment as the imposed strain speed might not be constant during compaction or deviate from the prescriptions.

4. Conclusion

In this article, we validate the use of a non-linear variant of the three-branches Maxwell–Wiechert model with strain dependent stiffnesses and strain-rate dependent relaxation times as proposed by Danzi et al. [18] in order to model the compressive behaviour of several textiles as a function of strain and strain rate. We propose a method to numerically solve the model by linearizing it over small time intervals, allowing to calculate the textile response for any strain profile. We demonstrate that the model yields accurate results over a wide range of textile architectures and fibre volume fractions in both dry and wet conditions considering the large variability of fibre beds.

We present and validate a numerical method for parameter extraction overcoming simplifications usually met in analytical models such as a constant Young's modulus E_0 and an ideal strain profile. The parameter extraction is based on the measured strain profile rather than the prescribed one as both can differ due to machine deflection and actuation error. This method also enables model validation with any strain profile, which should be considered in future research. Because in the approach that we follow, presented by Danzi [18], only three parameters are optimized at once, the global minimum is not guaranteed to be found. In addition, it has not been established that the necessary and sufficient conditions for the simplex algorithm to find the global minimum are present. However, the quality of the fits that we present in this article proves the validity of the approach and suggests that the improvement provided by finding the global minimum is rather small.

The model presented here does not take into account any effects related to cyclic compaction, which have a direct influence on the

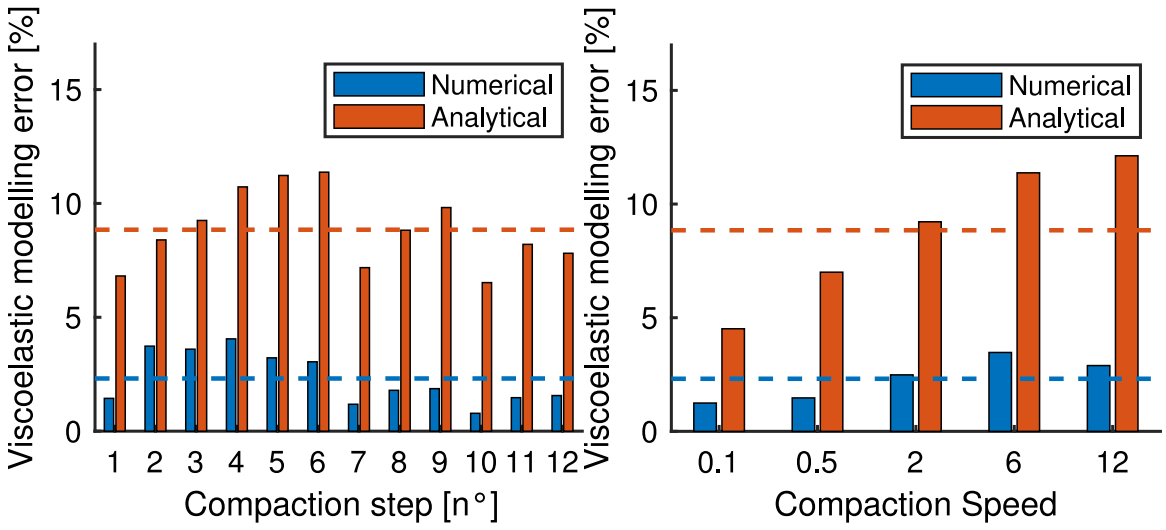

Fig. 15. Viscoelastic modelling error with parameters extracted based on the measured (numerical) and assumed (analytical) strain for the carbon plain weave in dry condition. Fig. 15(a) shows the viscoelastic modelling error over the compaction steps and Fig. 15(b) over the compaction speed . The dashed line is the overall mean viscoelastic modelling error.

textile compaction response [12], and therefore only applies to textiles which have not been subjected to multiple compaction/ decompaction cycles. The model is rather intended for processes where the textile will be subjected to a single compaction such as encountered in CRTM or RFI. Processes with a wide range of strain, strain speeds and strain profiles can be modelled. Regarding that, the influence of the compaction history on the results should be quantified in future work to evaluate its effect, which may probably very much depend on the textile architecture. It remains to be verified if the developed model remains valid for relaxation, which would enables other applications such as direct thermoplastic melt infusion.

We observe that the measured strain profile differs from the prescribed one in terms of total strain and strain rate, moreover the strain rate is not perfectly constant during compaction. We show that strain deviations resulting from machine compliance and actuation error have an important impact that can skew the viscoelastic parameter extraction if not considered, resulting in incorrect modelling of fibre beds stress response. This is detrimental for the manufacturing techniques which require knowledge about the fibre bed stress response such as CRTM [1,2], RFI [3–5] or direct thermoplastic melt impregnation [6,7]. We find that the viscoelastic modelling error drastically decreases when considering strain deviations, and therefore advocate for the necessity of doing so. Another consequence of these results is that strain deviations in the tool should be considered during manufacturing.

Because the measurements are so sensitive on the tool distance and strain, LVDT or more accurate methods such as proposed by Sousa and al. should be used. Further improvements on the model include for instance the consideration of fluid pressure in fast compaction similar to the method proposed by Saunders [29]. Saunders investigated the fluid pressure in unperforated plates where the flow takes place in-plane. In this study the perforated bottom plate allows fluid evacuation at the bottom of the sample additionally to the sides and the flow mainly takes place in the through-thickness direction. The fluid pressure build-up is much smaller in that case because of the shorter flow lengths. However, at very high compaction speeds and elevated loads, which are significantly decreasing the ability of the fluid to flow in a time-scale comparable to the experiment, the pressures might not be completely safe to neglect and this issue should be examined in future work. Besides the flow lengths, the pressure build up also depends on the through-thickness permeability of the textile so that textiles with a lower permeability are more sensitive to such effects. Additionally, it should be investigated if actuating the crosshead during relaxation such as to keep the cavity height constant is feasible. The very accurate actuation required at elevated loads might be beyond the capabilities of the actual testing machines so that actuation error might still remain a burden that cannot be completely eliminated and needs to be dealt with. However, the actuation of submicron-milling machines or atomic-force microscopes is very precise but probably quite expensive. Finally, an analysis of the influence of actuation error on the measurements can be repeated with other models or fields using similar methods.

CRediT authorship contribution statement

Vincent Werlen: Conceptualization, Methodology, Software, Validation, Formal analysis, Investigation, Writing - original draft, Visualization. **Christian Rytka:** Resources, Writing - review & editing, Supervision, Project administration. **Véronique Michaud:** Writing - review & editing, Supervision.

Declaration of competing interest

The authors declare that they have no known competing financial interests or personal relationships that could have appeared to influence the work reported in this paper.

Acknowledgements

This work is part of the research project Consolidation of Thermoplastic hybrid yarn materials “ConThP” and is funded by the German Research Foundation [394279584] and the Swiss National Science Foundation [200021E/177210/1]. We would like to thank the collaborators of the “ConThP” project for their precious support: Clemens Dransfeld, Christian Brauner, Richard Vocke and Philipp Schwanemann.

References

[1] Bhat P, Merotte J, Simacek P, Advani SG. Process analysis of compression resin transfer molding. Composites A 2009;40(4):431–41.

[2] Bachmann B, Masania K, Dransfeld C. Simulation of the compression resin transfer moulding process for high volume manufacturing. In: TexComp-11. Leuven. 2013.

[3] Park J, Kang MK. A numerical simulation of the resin film infusion process. Compos Struct 2003;60(4):431–7.
[4] Jespersen ST, Wakeman MD, Michaud V, Cramer D, Månson J-AE. Film stacking impregnation model for a novel net shape thermoplastic composite preforming process. Compos Sci Technol 2008;68:1822–30.
[5] Cender TA, Simacek P, Advani SG. Resin film impregnation in fabric prepregs with dual length scale permeability. Composites A 2013;53:118–28.
[6] Studer J, Dransfeld C, Fiedler B. Direct thermoplastic melt impregnation of carbon fibre fabrics by injection moulding. In: ECCM17. Munich, Germany. 2016.
[7] Studer J, Dransfeld C, Cano JC, Keller A, Wink M, Masania K, et al. Effect of fabric architecture, compaction and permeability on through thickness thermoplastic melt impregnation. Composites A 2019;122:45–53.
[8] Van Wyk CM. Note on the compressibility of wool. J Text Inst Trans 1946.
[9] Kelly PA. A viscoelastic model for the compaction of fibrous materials. J Text Inst 2011;102(8):689–99.
[10] Somashekar AA, Bickerton S, Bhattacharyya D. Modelling the viscoelastic stress relaxation of glass fibre reinforcements under constant compaction strain during composites manufacturing. Composites A 2012;43(7):1044–52.
[11] Vangheluwe L, Kiekens P. Modelling relaxation behaviour of yarns part I: Extended, nonlinear maxwell model. J Text Inst 1996;87(2):296–304.
[12] Kabachi M, Danzi M, Arreguin S, Ermanni P. Experimental study on the influence of cyclic compaction on the fiber-bed permeability, quasi-static and dynamic compaction responses. Composites A 2019;125.
[13] Wolfrath J, Michaud V, Månson J-AE. Deconsolidation in glass mat thermoplastic composites: Analysis of the mechanisms. Composites A 2005;36:1608–16.
[14] Wolfrath J, Michaud V, Månson J-AE. Deconsolidation in glass mat thermoplastics: Influence of the initial fibre/matrix configuration. Compos Sci Technol 2005;65:1601–8.
[15] Servais C, Michaud V, Månson J-AE. The packing stress of impregnated fiber mats. Polym Compos 2001;22(2):298–311.
[16] Michaud V, Månson J-AE. Impregnation of compressible fiber mats with a thermoplastic resin. Part I: Theory. J Compos Mater 2001;35(13):1150–73.
[17] Michaud V, Törnqvist R, Månson J-AE. Impregnation of compressible fiber mats with a thermoplastic resin. Part II: Experiments. J Compos Mater 2001;35(13):1174–200.
[18] Danzi M, Schneeberger C, Ermanni P. A model for the time-dependent compaction response of woven fiber textiles. Composites A 2018;105:180–8.
[19] Toll S. Packing mechanics of fiber reinforcements. Polym Eng Sci 1998;38(8):1337–50.
[20] Kim YR, Mccarthy SP, Fanucci JP. Compressibility and relaxation of fiber reinforcements during composite processing. Polym Compos 1991;12(1):13–9.
[21] Wei K, Liang D, Mei M, Yang X, Chen L. A viscoelastic model of compression and relaxation behaviors in preforming process for carbon fiber fabrics with binder. Composites B 2019;158:1–9.
[22] Bickerton S, Buntain MJ, Somashekar AA. The viscoelastic compression behavior of liquid composite molding preforms. Composites A 2003;34(5):431–44.
[23] Yong AXH, Aktas A, May D, Endruweit A, Lomov SV, Advani SG, et al. Experimental characterisation of textile compaction response: a benchmark exercise. Composites Part A: Applied Science and Manufacturing 2021 142:106243.
[24] Sousa P, Lomov SV, Ivens J. Methodology of dry and wet compressibility measurement. Composites A 2020;128(August 2019):105672.
[25] Gutowski TG, Cai Z, Bauer S, Boucher D, Kingery J, Wineman S. Consolidation experiments for laminate composites. J Compos Mater 1987;21:650–69.
[26] Papanicolaou G, Zaoutsos S. Viscoelastic constitutive modeling of creep and stress relaxation in polymers and polymer matrix composites. In: Creep and fatigue in polymer matrix composites. 2nd ed.. Woodhead Publishing; 2019.
[27] Murty K. Linear programming. John Wiley & Sons; 1983.
[28] Robitaille F, Gauvin R. Compaction of textile reinforcements for composites manufacturing. I: Review of experimental results. Polym Compos 1998;19(2):198–216.
[29] Saunders R, Lekakou C, Bader M. Compression in the processing of polymer composites 2. Modelling of the viscoelastic compression of resin-impregnated fibre networks. Compos Sci Technol 1999;59:1483–94.